Eur. Phys. J. A (2023) 59:69
https://doi.org/10.1140/epja/s10050-023-00984-y

THE EUROPEAN PHYSICAL JOURNAL A

Regular Article - Experimental Physics

Measurement of total and partial cross sections of the ^{90}Zr(p,γ)^{91}Nb reaction with in-beam γ-ray spectroscopy

Philipp Erbacher[1], Tanja Heftrich[1], Anne Endres[1], Jan Glorius[2], Lars Netterdon[3], David Just[1], Kathrin Göbel[6], Milan Krtička[4], René Reifarth[1,5,a], Kerstin Sonnabend[1], Benedikt Thomas[1], Mario Weigand[1], Andreas Zilges[3]

[1] Goethe University Frankfurt, Max-von-Laue Str. 1, Frankfurt 60438, Germany
[2] GSI Helmholtzzentrum für Schwerionenforschung, Planck Str. 1, Darmstadt 64291, Germany
[3] University Cologne, Zülpicher Straße 77, Cologne 50937, Germany
[4] Charles University, Prague, Czech Republic
[5] University of Notre Dame, Notre Dame 46556, IN, USA
[6] Facility for Antiproton and Ion Research in Europe GmbH, Planck Str. 1, Darmstadt 64291, Germany

Received: 16 November 2022 / Accepted: 16 March 2023

Communicated by Wolfram Korten

Abstract The origin of many p-nuclei remains an unsolved problem in nuclear astrophysics. While photo-dissociation reactions in the γ-process can explain the production of many p-nuclei, some, notably ^{92,94}Mo and ^{96,98}Ru are underproduced in network calculations. The ^{90}Zr(p,γ)^{91}Nb reaction is part of a possible (p,γ) reaction chain for the production of the p-nucleus ^{92}Mo. Available data show a large disagreement between the different reported cross sections measurements for the ^{90}Zr(p,γ)^{91}Nb reaction. We measured proton capture cross sections with an enriched ^{90}Zr target using in-beam γ-ray spectroscopy for proton energies between 2.75 MeV and 5.1 MeV. The emitted γ-rays were detected using the HORUS (**H**igh efficiency **O**bservatory for γ-**R**ay **U**nique **S**pectroscopy) detector array at the University of Cologne, Germany. To account for the possible contribution of the ^{91}Zr(p,n) reaction, an enriched ^{91}Zr was irradiated. We measured production cross sections for the ground and isomeric state of ^{91}Nb as well as partial cross section for up to ten high-energy primary transitions. The results are in good agreement with a former in-beam γ-ray spectroscopy measurement by Laird et al.. We provide a possible explanation for the discrepancies between our data and other available measurements.

1 Astrophysical motivation

Heavy isotopes are mainly produced by neutron capture reactions in the so-called s- and r-process [1]. However 35 nuclei in the mass region between Se and Hg are shielded from the s- and r-process by stable nuclei [2,3]. The process and production scenario for these p-nuclei is an ongoing research topic. Different scenarios like Type II Supernovae, Type Ia supernovae, neutrino-driven winds during core-collapse supernovae and hydrogen burning on the surface of accreting neutron stars have been investigated [4–7].

A promising scenario takes place in Type II supernovae when the shock wave passes through the O/Ne layer of the star and temperatures of $2 < T < 3$ GK are reached [6]. Under these conditions the γ-flux and temperatures are high enough to photodissociate heavy nuclei, which were earlier produced in the s- and r-process, by a combination of (γ,n), (γ,p) and (γ,α) reactions. The observed abundances can mainly be explained by this so-called γ-process, but some isotopes, notably ^{92,94}Mo and ^{96,98}Ru, are heavily underproduced in reaction network calculations [8]. This could be the result of our limited understanding of the stellar conditions during p-process nucleosynthesis and uncertainties of the physical input parameters used to calculate the relevant stellar reaction rates [3,9].

Some authors also suggested a significant contribution of (p,γ) reactions for the production of the light p-nuclei. To quantify these contributions, a good understanding of the involved reaction rates is important (Fig. 1). One important reaction in the reaction chain leading to ^{92}Mo is the proton capture on ^{90}Zr. The ^{90}Zr(p,γ)^{91}Nb reaction has been investigated multiple times, but the results show significant discrepancies.

Laird et al. [11] used in-beam γ-ray spectroscopy to measure the cross section with two Ge(Li) detectors placed at 135° and 165° relative to the proton beam. From these measurements they inferred the total γ-yield for the dominant

[a] e-mail: reifarth@physik.uni-frankfurt.de (corresponding author)

Published online: 04 April 2023

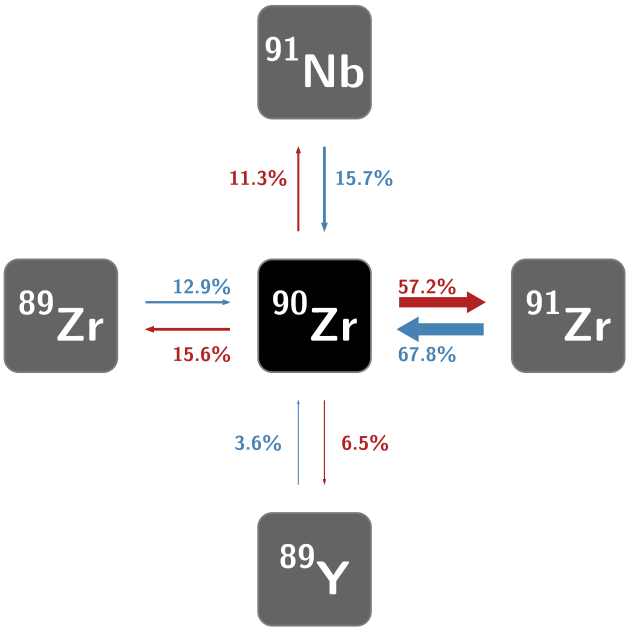

Fig. 1 Nucleosynthesis production (blue) and destruction (red) reaction flows for ^{90}Zr during a Supernova type II [8,10]. The sum of all production fluxes is normalized to 100%, and the destruction fluxes are scaled with the same factor. With 67.8%, the strongest reaction contributing to ^{90}Zr is ^{91}Zr(γ,n) (blue arrow to the left). The strongest destruction reaction is ^{91}Zr(n,γ) (red arrow to the right). About 11% of ^{90}Zr is destroyed via proton capture (red arrow upwards). Fluxes smaller than 1% are not shown

transitions ending in the ground and isomeric states of ^{91}Nb to obtain the total proton capture cross section.

Roughton et al. [12] measured the astrophysical reaction rate directly via the activation technique by irradiating a thick zirconium target. These measurements cannot be compared directly to cross sections measured by Laird et al., but comparisons using theoretical prediction show that both measurements are in disagreement, especially for proton energies above 3 MeV. To solve this discrepancy, Spyrou et al. [13] measured the cross sections using the γ-summing technique with a NaI based calorimetric detector [13] They showed, using predictions by the NON-SMOKER code [14], that their data are in agreement with the thick-target yield measurements of Roughton et al. [12].

Since the in-beam γ-ray spectroscopy measurement by Laird et al. seems to be the outlier, we decided to measure the ^{90}Zr(p,γ) cross section again using the same technique to verify the results.

2 Experiment

2.1 Experimental setup

The experiment was performed using a 10 MV tandem ion accelerator at the Institute for Nuclear Physics at the University of Cologne, Germany. An array of HPGe detectors called HORUS (**H**igh efficiency **O**bservatory for γ-**R**ay Unique **S**pectroscopy) measured the prompt γ-rays emitted after the reaction at five different angles with respect to the beam axis [15]. Up to 14 detectors can be mounted to the HORUS spectrometer of which six can be equipped with bismuth germanate shields (BGO) for background suppression. For our measurement only 13 HPGe detectors were used, since one detector was replaced by a silicon Rutherford backscattering detector (RBS) to monitor the target condition during the experiment [15]. The detectors were placed at five angles (35°, 45°, 90°, 135°, and 145°) relative to the proton beam axis [15]. A γ-ray spectrum for a proton energy of $E_p = 5.1$ MeV at 90° is shown in Fig. 2.

A thin zirconium foil enriched in ^{90}Zr (97.65 ± 0.10)% and an areal density of (534 ± 27) μg/cm^2 was used. The enriched target still contained (0.98 ± 0.05)% of ^{91}Zr. To disentangle possible contributions of the ^{91}Zr(p,n) reaction from the measured cross section, a second target, enriched in ^{91}Zr (89.20 ± 0.10)% with an areal density of (530 ± 45) μg/cm^2 was also irradiated. The areal density of the targets was measured at three different positions using the Rutherford Backscattering technique at the RUBION facility at the Ruhr-University Bochum, Germany. We used the program SIMNRA to calculate the energy distribution of the backscattered α-particles for different target thicknesses and fit the measured spectra [16]. The areal density of the enriched ^{91}Zr targets varied between 484 μg/cm^2 and 576 μg/cm^2 resulting in an average thickness of 530 μg/cm^2 and a higher uncertainty compared to the ^{90}Zr target where the thickness was the same within the margin of error for all measured positions. The areal densities for both targets are tabulated in Table 1. The irradiated targets were measured again at RUBION after the first beam time and no degradation was observed.

A thick gold backing stopped the proton beam behind the target where the total deposited charge was measured to determine the total proton flux on the target for each irradiation. Additionally, the charge collected by the target chamber was measured to account for secondary electrons. A negatively charged aperture (U = − 400 V) prevented the secondary electron from leaving the target chamber. The total

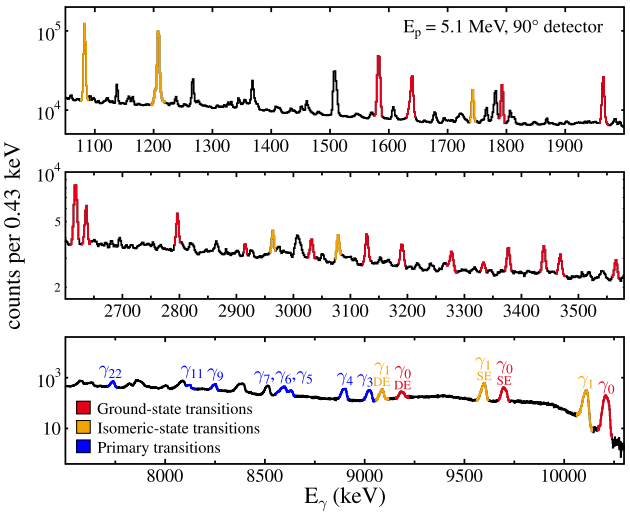

Fig. 2 γ-ray spectrum for irradiation of the ^{90}Zr target with protons for a beam energy of 5.1 MeV. Transitions ending in the ground and isomeric state at 104 keV of ^{91}Nb are marked in red and orange, respectively. The high-energy primary transitions into the ground state (γ_0), first excited state (γ_1), as well as higher excited states are marked. The final level for each primary transition can be found in Table 3. The single escape (SE) and double escape peaks (DE) for γ_0 and γ_1 are also marked. The unmarked peaks are either background peaks, transitions which do not end in the ground or isomeric state, or SE and DE peaks

uncertainty of the current readout amounts to 5%.

Data were taken over the course of two measurement campaigns. During the first experiment, the targets were irradiated at six proton energies between 3.5 MeV and 5.1 MeV. We also performed measurements with only the gold backing for each beam setting to account for contribution of protons reacting in the backing. One year later three proton energies between 2.75 MeV and 3.3 MeV were measured. The 5.1 MeV irradiation was performed twice to check for possible discrepancies between both campaigns.

2.2 Characterisation of the proton beam

The energy calibration of the proton beam was checked by scanning the $E_p = 3674.4$ keV resonance of the ^{27}Al(p,γ)^{28}Si reaction measured by Brenneisen et al. [17]. The method is based on the procedure described by Netterdon et al. [18]. The γ-yield of the 1779 keV transition into the ground state of ^{28}Si was measured for different magnet settings in step sizes between 0.5 and 1 keV. The γ-yield is roughly constant for energies below the resonance energy and increases by a factor of about two at the resonance energy. Since protons lose energy in the target, no well defined resonance peak can be observed, but rather a resonance plateau. The observed position of the resonance and the energy spread of the proton beam of ± 3 keV was calculated from the rise of the yield curve. The difference between the observed and the expected position of the resonance is the offset of the magnet. This offset was found to be (27.14 ± 1.01) keV.

Because of the energy loss in the target, the average proton energy of captured protons is smaller than the measured beam energy. The energy loss was simulated using Geant4 [19] and SRIM [20]. Both simulations agree within 2–3%. The average calculated energy loss in the ^{90}Zr target was in the range of 21.5 keV to 31.30 keV depending on beam energy. The average energy loss in the middle of the target was used to calculate the average center-of-mass energy. Since the enriched ^{90}Zr and ^{91}Zr targets have slightly different thicknesses, the average energy loss differs by about 4 keV. The effect of this difference in energy loss is expected to be negligible because the proton capture cross section does not change significantly in such a small energy range.

2.3 Determination of the full-energy peak efficiency

The full-energy peak efficiency of individual HPGe detectors has to be known over the measured photon energy range from 1.0 to 10.5 MeV. A three step approach was used for the efficiency determination. First, the absolute full-energy

Table 1 Isotopic composition and areal density for the enriched ^{90}Zr and ^{91}Zr targets

Isotope	^{nat}Zr	^{90}Zr target		^{91}Zr target	
	Abundance [%]	Abundance [%]	Areal density [μg/cm^2]	Abundance [%]	Areal density [μg/cm^2]
^{90}Zr	51.45 ± 0.40	97.65 ± 0.10	521 ± 26	5.99 ± 0.10	31.8 ± 2.8
^{91}Zr	11.22±0.05	0.98 ± 0.05	5.13 ± 0.37	89.20 ± 0.10	472 ± 40
^{92}Zr	17.15 ± 0.08	0.71 ± 0.05	3.79 ± 0.33	3.29 ± 0.05	17.4 ± 1.5
^{94}Zr	17.38 ± 0.28	0.55 ± 0.05	2.94 ± 0.31	1.30 ± 0.05	6.89 ± 0.64
^{96}Zr	2.80 ± 0.09	0.13 ± 0.05	0.69 ± 0.27	0.23 ± 0.05	1.22 ± 0.28

The areal density was measured using Rutherford Backscattering Spectrometry at the RUBION facility at the Ruhr-University Bochum, Germany. The isotopic abundances were taken from the data sheet provided by the manufacturer

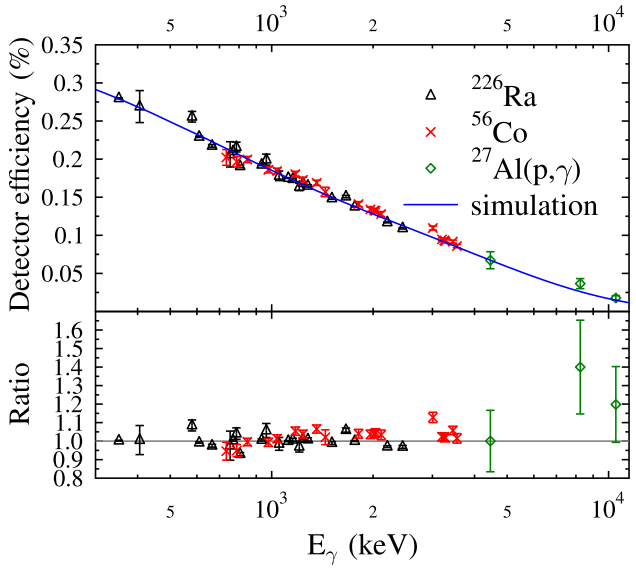

Fig. 3 Full-energy-peak efficiency for one of the HPGe detectors at 90°. ^{226}Ra and ^{56}Co sources were used to measure efficiencies up to 3.5 MeV. The relative intensities of the three strongest γ-rays (4458 keV, 8239 keV and 10509 keV) from the 3674.4 keV resonance were measured by Brenneisen et al. and used to obtain the relative efficiency of the detector up to 10.5 MeV [17]. The efficiencies were simulated using Geant4 [19]. The ratio of measured efficiencies to the simulated efficiency curve is shown in the lower panel

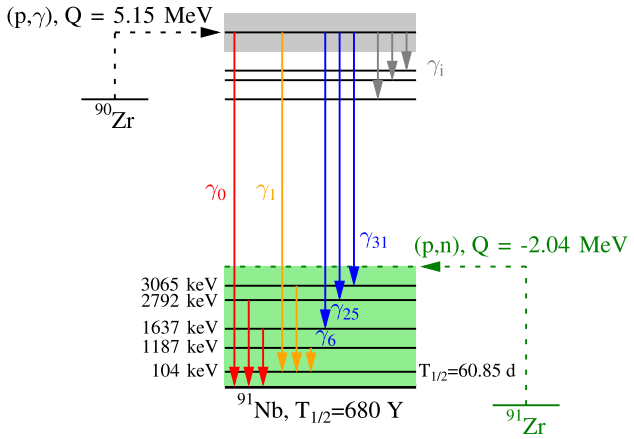

Fig. 4 Simplified reaction scheme for the ^{90}Zr(p,γ) and ^{91}Zr(p,n) reactions. After the proton capture (and neutron emission from ^{92}Nb) an excited nucleus of ^{91}Nb is formed, which de-excites through the emission of γ-rays until its ground or isomeric state is reached. The primary γ-rays (from radiative capture) to a low lying state i are labeled as γ_i. The maximum excitation energy of the ^{91}Nb state formed via the ^{91}Zr(n,p) reaction is about 7.2 MeV lower compared to the ^{90}Zr(p,γ) reaction. Since the neutron can carry some or all of the energy, the entry state is not clearly defined. The excitation energies of shown levels were adopted from Ref. [21]

peak efficiency up to $E_\gamma \approx 2.5$ MeV was determined using a calibrated ^{226}Ra source. To extend this energy range up to $E_\gamma \approx 3.5$ MeV, an uncalibrated ^{56}Co source was used. The relative efficiency of the ^{56}Co measurement was scaled to the absolute efficiencies using the $E_\gamma \approx 846.77$ keV transition of the ^{56}Co decay. We simulated the whole HORUS detector setup using Geant4 [19] to obtain detector efficiencies up to 10.5 MeV. We used the strongest γ-ray transitions (4458 keV, 8239 keV and 10,509 keV) of the ^{27}Al(p,γ) resonance at 3674.4 keV to check the energy dependency of the simulated cross sections. The measured and simulated efficiencies and their ratios are shown in Fig. 3 for one of the 90° detectors. The simulated efficiencies were used for further analysis.

3 In-beam γ-ray spectroscopy

A direct method to measure proton capture cross sections is the in-beam γ-ray spectroscopy. When a proton reacts with a ^{90}Zr nuclei, a ^{91}Nb nucleus is formed with an excitation energy equal to the sum of the Q-value of the ^{90}Zr(p,γ) reaction, $Q = 5.15$ MeV, and the center of mass energy $E_{\mathrm{c.m.}}$ of the system. The ^{91}Nb formed by proton capture de-excites by a γ-ray cascade until it's ground or isomeric state at 104 keV ($t_{1/2} = 60.86$ d [21]) is reached. A simplified reaction scheme is shown in Fig. 4. The total production cross section σ^i_{pro} of any level i of ^{91}Nb can be determined as the sum of partial cross sections of all γ-rays emitted by all levels k with higher excitation energies and ending at level i.

$$\sigma^i_{\mathrm{pro}} = \sum_{k>i} \sigma^{k\to i} = \sum_{k=0}^{N} \frac{A^{k\to i}}{n_t N_p \varepsilon_\gamma^{k\to i}} \tag{1}$$

with the total number of detected γ-rays $A_k^{k\to i}$, the detector efficiency for the γ-ray $\varepsilon_\gamma^{k\to i}$, the number of protons N_p and the areal density n_t of the target. We assumed that the level scheme of ^{91}Nb, including decays of individual levels, is known up to excitation energy of 4 MeV. The partial cross section for all transitions in this region or at least those feeding the ground and first excited state could be determined from individual peaks observed in the measured spectra. Contribution of transitions from higher excitation energies has to be estimated. This estimation was made using a modified version of the DICEBOX code [22], see Sect. 4.

3.1 Angular distribution

The angular distribution of the emitted γ-rays has to be taken into account for the calculation of $\sigma^{k\to i}$. The angular distribution of the γ-rays were measured at five different angles relative to the proton beam. As mainly dipole ($k = 2$) and quadrupole ($k = 4$) transitions play a role in the γ decay, the $\sigma_{p\gamma}^{k\to i}(\vartheta)$ was considered in the form:

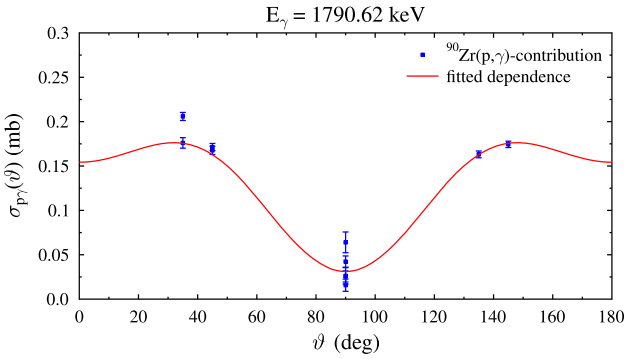

Fig. 5 Angular distribution of the cross section for the 1790 keV transition into the ground state of ^{91}Nb at different angles relative to the proton beam direction for $E_p = 5100$ keV. The fit of experimental data is shown as the red line

$$\sigma_{p\gamma}^{k\to i}(\vartheta) = \sigma_{p\gamma}^{k\to i}\left(1 + \sum_{j=2,4} \alpha_j^{k\to i} P_j(\cos(\theta))\right) \tag{2}$$

with the legendre polynomial P_k and the fit parameter $\alpha_j^{k\to i}$. An example for the 1790 keV transition into the ground state of ^{90}Zr is shown in Fig. 5 for a beam energy of $E_p = 5.1$ MeV.

3.2 Contributions from the ^{91}Zr(p,n) reaction

The ^{90}Zr target used for the experiment was not isotopically pure and contained 0.96% of ^{91}Zr. Since the ^{91}Zr(p,n) reaction also produces ^{91}Nb, but with a 2–20 times higher cross section within the measured energy range, the contribution of the ^{91}Zr(p,n)-reaction has to be taken into account. The contribution from the ^{91}Zr(p,n) was determined by measuring a target enriched in ^{91}Zr for each beam energy.

The number of photons $N_{p\gamma+pn}^{k\to i}$ detected at an angle ϑ for a transition from state k to state i can be divided in the contributions of the ^{90}Zr(p,γ) and ^{91}Zr(p,n) reactions, labeled via subscripts pγ and pn, respectively:

$$N_{p\gamma+pn}^{k\to i}(\vartheta) = N_{p\gamma}^{k\to i}(\vartheta) + N_{pn}^{k\to i}(\vartheta) \tag{3}$$

These contributions can individually be written as:

$$\begin{aligned} N_{p\gamma}^{k\to i}(\vartheta) &= \sigma_{p\gamma}^{k\to i}(\vartheta)\epsilon_\gamma I_{p\gamma} n_t N_p \\ N_{pn}^{k\to i}(\vartheta) &= \sigma_{pn}^{k\to i}(\vartheta)\epsilon_\gamma I_{pn} n_t N_p \end{aligned} \tag{4}$$

with the angular-dependent partial cross section $\sigma_{p\,\gamma}^{k\to i}(\vartheta)$ and $\sigma_{pn}^{k\to i}(\vartheta)$, the isotopic abundance fraction $I_{p\gamma}$ and I_{pn} of ^{90}Zr and ^{91}Zr in the target, the full energy peak efficiency ϵ_γ, target areal density n_t and the number of protons hitting the target N_p.

Combining Eqs. 3 and 4 and solving for $\sigma_{p\gamma}^{k\to i}$ yields the angular dependent cross sections for the ^{90}Zr(p,γ) reaction.

$$\sigma_{p\gamma}^{k\to i}(\vartheta) = \frac{\frac{N_{p\gamma+pn}^{k\to i,1}(\vartheta)}{n_t^1 N_p^1} - \frac{N_{p\gamma+pn}^{k\to i,2}(\vartheta) I_{pn}^1}{n_t^2 N_p^2 I_{pn}^2}}{\epsilon_\gamma (I_{p\gamma}^1 - \frac{I_{p\gamma}^2}{I_{pn}^2} I_{pn}^1)} \tag{5}$$

The correction to the measured cross section resulting from this contribution is different for each transition and proton energy and varies between 0% and about 10%. Due to the lower Q-value of the ^{91}Zr(p,n) reaction of $Q = -2.04$ MeV, the maximum excitation energy is lower compared to the ^{90}Zr(p,γ) reaction. For proton energies below $E_p = 3263$ keV, the excitation energy is not high enough to reach the second excited level of ^{91}Nb at 1186.88 keV and no transition has a contribution from the ^{91}Zr(p,n) reaction.

4 Contributions from unobserved transitions

The level scheme of ^{91}Nb is well known only up to an excitation energy of about 4 MeV. The highest level from which transitions in the ground or isomeric state were observed for all proton energies, was at 2792 keV. To estimate the contribution of all γ-ray transitions from higher-lying levels of ^{91}Nb above 2792 keV we exploited γ-ray cascades modeled with a modified version of DICEBOX code [22]. The input parameters needed for these calculations were models of photon strength functions (PSFs), nuclear level density (NLD) and spin and parity dependence of the initial states of ^{91}Nb formed by proton capture.

In practice, we first compared predictions of the cross section for the several primary transitions (those with sufficient statistics) using the TALYS code [22] for several different models of PSF, NLD and optical model potential. The comparison of these predictions with the best found combination of these models are shown in Fig. 9. This combination consists of the Hartree-Fock-Bogoluybov model with Gogny interaction (ldmodel =5) and semi-microscopic Hartree-Fock BCS model for electric dipole PSF (strength = 3). Default values were used for all other TALYS inputs.

The same models of PSF and NLD were then used in the DICEBOX simulations of the γ cascades. The adopted distribution of the spin and parity of initial states for each E_p was then also derived from the above-mentioned TALYS model. The advantage of using DICEBOX over TALYS for simulation of the γ decay is its possibility to get expected fluctuations of transitions intensities. The expectation value as well as standard deviation of the contribution of unknown transitions from excitation energies above 2792 keV feeding directly the ground or isomeric states were obtained from simulations of 500 different artificial nuclei (with 10^5 cascades simulated in each). The dependence of calculated frac-

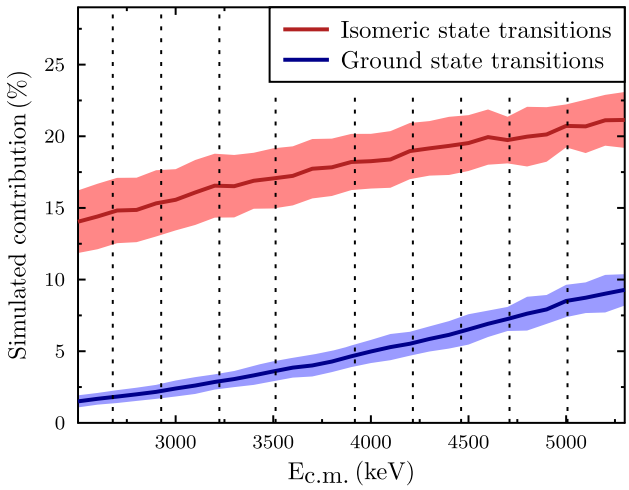

Fig. 6 Relative contribution of transitions from excitation energies above 4 MeV to the production cross section of the ground (blue) and isomeric (red) states based on DICEBOX predictions. The uncertainties correspond to one standard deviation. All measured proton energies are marked in dotted lines [22]

tion on the proton energy is shown in Fig. 6. We note that the distribution of the intensity from individual artificial nuclei gives a distribution that is very close to a normal distribution.

5 Results

5.1 Production cross sections

We determined the ^{90}Zr(p,γ) production cross sections populating the ground and isomeric states of ^{91}Nb. The results are given in Table 2. We list here the observed cross section corresponding to transitions from excitation energies below 4 MeV and the corresponding primary transition as well as the cross section that includes the correction for the transitions from higher excitation energies.

The statistical uncertainties range from 1 to 3% resulting mainly from the fit of the angular distribution for each transition. The systematic uncertainties amount to 10% resulting from the detector efficiencies (5%), the charge measurement to determine the total number of protons impinging on the target (5%) and the target areal density (7%). The total radiative proton capture cross sections are compared to literature values and prediction by NON-SMOKER [14] and TALYS−1.95 [23] in Fig. 7. For TALYS, we used models of PSFs and NLD and optical model potential mentioned in Sect. 4.

Our cross sections agree with a former in-beam γ-ray spectroscopy measurement by Laird et al. [11], but show an increasing divergence from the calorimetric measurement by Spyrou et al. [13] for $E_p > 3500$ keV. The thick-target yield measurement by Roughton et al. [12] cannot be com-

Table 2 Cross sections for the ^{90}Zr(p,γ)^{91}Nb^{iso} (isomer), ^{90}Zr(p,γ)^{91}Nb^{ground} (ground state), ^{90}Zr(p,γ)^{91}Nb^{tot} (total) reactions for all measured beam energies

$E_{c.m.}$ keV	σ_{ground} μb	σ_{iso} μb	σ_{total} μb
2678 ± 16	24.3 ± 0.4	126 ± 2	151 ± 3
	24.7 ± 5.9	**148** ± 23	**173** ± 24
2926 ± 15	48.0 ± 0.9	215 ± 4	263 ± 5
	49.2 ± 11.5	**255** ± 35	**304** ± 37
3224 ± 14	107 ± 2	343 ± 5	451 ± 7
	111 ± 20	**411** ± 55	**522** ± 58
3521 ± 13	203 ± 6	503 ± 13	706 ± 18
	211 ± 39	**607** ± 75	**818** ± 85
3918 ± 12	471 ± 8	886 ± 17	1360 ± 30
	495 ± 81	**1080** ± 120	**1580** ± 140
4215 ± 12	537 ± 8	1120 ± 19	1660 ± 30
	570 ± 86	**1380** ± 140	**1950** ± 170
4462 ± 11	864 ± 10	1440 ± 10	2300 ± 20
	925 ± 147	**1780** ± 180	**2710** ± 231
4710 ± 11	1250 ± 13	1960 ± 20	3220 ± 30
	1350 ± 191	**2450** ± 240	**3810** ± 300
5007 ± 10	1220 ± 20	2340 ± 20	3550 ± 25
	1330 ± 170	**2950** ± 250	**4280** ± 300
5045 ± 10	1340 ± 30	2240 ± 40	3580 ± 60
	1470 ± 180	**2820** ± 260	**4290** ± 320

The average beam energy at the middle of the target and the energy spread is given. The energy spread was calculated from using the energy width of the proton beam and half of the average energy loss in the target. The measured section from observed well-resolved transitions as well as the cross section corrected for the contribution of the transitions from excitation energies above 4 MeV (bold values) are given, for details see Sect. 4. The systematic uncertainty is 10%, see Sect. 5.1

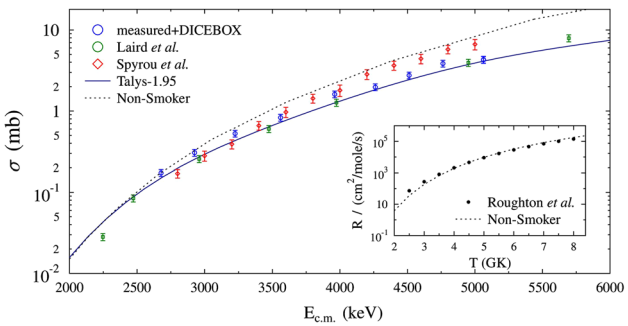

Fig. 7 Our cross sections for the ^{90}Zr(p,γ)^{91}Nb^{tot} reaction compared to data published by Laird et al. [11], Roughton et al. [12] and Spyrou et al. [13]. The experimental data are in agreement below $E_{c.m.} = 3500$ keV, but for higher energies the data of Spyrou et al. are diverging from our and Laird et al. data. The reaction rates measured by Roughton et al. are in agreement with the NON-SMOKER predictions [14]. For TALYS the optimized models mentioned in Sect. 4 were used

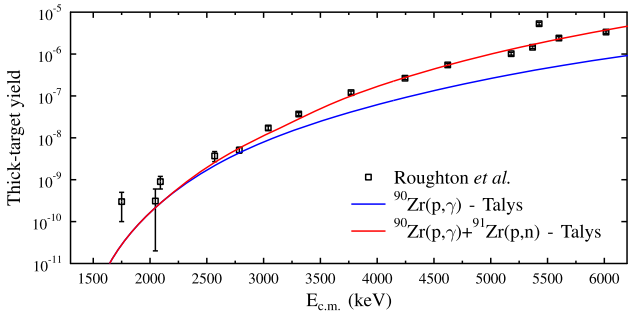

Fig. 8 The thick-target yields calculated using TALYS−1.95 predictions compared to yields measured by Roughton et al. [12]. A natural zirconium target was assumed for the calculation. See Sect. 5.2 for details

pared directly, since they only measured the total yield and used it to calculate the astrophysical reaction rate R (for several different stellar temperatures). However the prediction of NON-SMOKER for the reaction rate and the cross section can be used to compare the results. Based on these predictions Roughton et al. measurement also diverges from our results for $E_p > 3500$ keV.

5.2 Discussion of the discrepancies

Of the four available measurements, only our measurement and the second in-beam γ-ray spectroscopy by Laird et al. are in good agreement over the entire measured energy range. The discrepancy between the activation measurement by Roughton et al. and the in-beam γ-ray spectroscopy measurements can easily be explained by an unaccounted contribution from the ^{91}Zr(p,n) reaction during the activation measurement. Roughton et al. did not provide any information about the isotopic abundance of the used zirconium target nor was any correction for the ^{91}Zr(p,n) contribution above 3 MeV mentioned. We assume, therefore, a natural composition of the Zr target (^{90}Zr: 51.45%, ^{91}Zr: 11.22%). Under this assumption the expected thick-target yield can be calculated using theoretical cross section from TALYS−1.95 for the ^{90}Zr(p,γ) and ^{91}Zr(p,n) reaction. The models described in Sect. 4 were used. The total theoretical thick-target yield for a thick natural zirconium target is shown in Fig. 8 compared to the yield measured by Roughton et al.. The results of Roughton et al. can be nicely reproduced if both the ^{90}Zr(p,γ) and ^{91}Zr(p,n) reactions are taken into account.

We can only speculate about the cause of the deviation between the data gained via the γ-summing technique by Spyrou et al. [13] and our measurement. Enriched ^{90}Zr targets have been used in both experiments. The deviation starts at beam energies around 3 MeV and increases toward higher energies. This again indicates a contribution of the ^{91}Zr(p,n)^{91}Nb reaction in data from Ref. [13].

Table 3 Partial cross sections of primary transitions for the ^{90}Zr(p,γ)

E$_{c.m.}$ keV	0 keV, $\frac{9}{2}+$ $\sigma(\gamma_0)$/μb	104 keV, $\frac{1}{2}-$ $\sigma(\gamma_1)$/μb	1186 keV, $\frac{5}{2}-$ $\sigma(\gamma_3)$/μb	1312 keV, $\frac{3}{2}-$ $\sigma(\gamma_4)$/μb	1581 keV, $(\frac{7}{2}+)$ $\sigma(\gamma_5)$/μb
2678 ± 16	2.5 ± 0.1	33.9 ± 1.8			
2926 ± 15	8.5 ± 0.4	64.3 ± 3.5			
3224 ± 14	5.0 ± 0.2	66.2 ± 3.6	24.3 ± 1.3		
3521 ± 13	16.8 ± 1.3	48.9 ± 3.6	35.5 ± 2.5	41.9 ± 2.9	
3918 ± 12	49.8 ± 3.8	89.5 ± 7.0	60.6 ± 4.1	58.6 ± 3.9	26.7 ± 1.7
4215 ± 12	43.2 ± 4.2	146 ± 16	56.2 ± 3.2	65.3 ± 4.1	36.5 ± 2.8
4462 ± 11	70.2 ± 5.8	89.1 ± 7.6	81.0 ± 0.6	115 ± 6	33.8 ± 1.8
4710 ± 11	99.9 ± 8.1	138 ± 11	90.1 ± 5.7	106 ± 2	60.7 ± 2.3
5007 ± 10	98.7 ± 7.8	132 ± 9	91.8 ± 6.4	100 ± 7	48.3 ± 1.3
5045 ± 10	135 ± 14	200 ± 16	117 ± 8	147 ± 8	68.7 ± 4.4
E$_{c.m.}$ keV	1612 keV, $\frac{3}{2}-$ $\sigma(\gamma_6)$/μb	1637 keV, $(\frac{9}{2}+)$ $\sigma(\gamma_7)$/μb	1844 keV, $(\frac{5}{2}-)$ $\sigma(\gamma_9)$/μb	1963 keV, $(\frac{5}{2}+)$ $\sigma(\gamma_{11})$/mb	2390 keV, $(\frac{3}{2}+)$ $\sigma(\gamma_{22})$/μb
3918 ± 12	34.4 ± 2.8	20.0 ± 0.9	33.8 ± 1.2		
4215 ± 12	41.8 ± 3.9	23.6 ± 2.4	31.9 ± 2.1	43.4 ± 1.3	22.4 ± 1.4
4462 ± 11	77.0 ± 5.3	26.8 ± 1.2	44.3 ± 2.2	48.5 ± 2.1	35.5 ± 1.5
4710 ± 11	71.0 ± 3.2	39.6 ± 3.9	78.4 ± 2.7	79.0 ± 3.8	52.9 ± 1.4
5007 ± 10	101 ± 6	38.3 ± 0.9	88.0 ± 3.7	75.2 ± 3.5	69.8 ± 1.5
5045 ± 10	106 ± 6	46.6 ± 4.8	95.6 ± 4.6	84.0 ± 3.9	62.2 ± 4.1

Only the statistical uncertainties are given. The systematic uncertainties for all data points are 10%

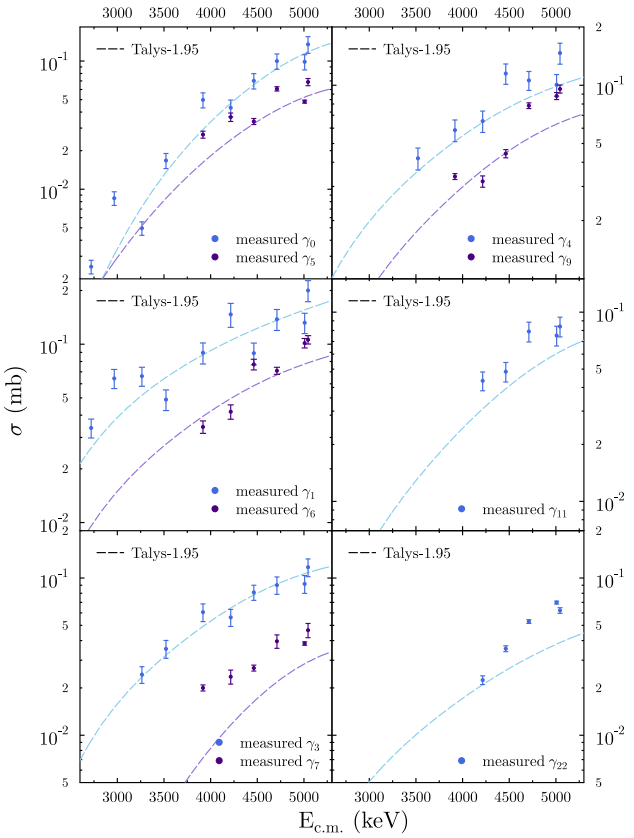

Fig. 9 Partial cross sections of primary transitions for the ^{90}Zr(p,γ) reaction. The data are compared to theoretical predictions by the Talys−1.95 code

5.3 Cross sections for primary transitions

We were able to determine cross sections of ten primary transitions from states formed by proton capture directly to lower lying excited states. Their cross sections are given in Table 3 and Fig. 9, where good agreement with TALYS predictions for the majority of transitions is also shown which further strengthens our interpretation of the deviation from the Roughton et al. data. Additional primary transitions were observed but were either to weak to be analysed or could not be reliably disentangled from peaks resulting from other transitions or their single and double escape lines.

6 Conclusions

Production cross sections for the ground and isomeric states of the ^{90}Zr(p,γ) reaction were measured at nine proton energies between 2700 keV and 5100 keV by means of in-beam γ-ray spectroscopy measuring individual transitions feeding these levels. A correction to unobserved transitions from high excitation energies was performed using statistical model. In addition the partial cross section for several primary transitions states were measured.

The results are in agreement with a former in-beam γ-ray spectroscopy measurement by Laird et al. [11]. The discrepancy with a previous thick-target yield measurement by Roughton et al. [12] can be explained assuming a contribution from the ^{91}Zr(p,n) reaction. In order to resolve this issue, the thick-target yield measurement should be repeated with two targets with different isotopic compositions to disentangle the possible contribution of the ^{91}Zr(p,n) reaction. The origin of the disagreement with the measurement by Spyrou et al. for higher proton energies is not clear.

Acknowledgements The authors thank A. Dewald and the accelerator staff at the Institute for Nuclear Physics at the University of Cologne and H. W. Becker of the Ruhr-University Bochum for the assistance on RBS measurements.

Funding Information Open Access funding enabled and organized by Projekt DEAL.

Data Availability Statement This manuscript has no associated data or the data will not be deposited. [Authors' comment: The data will be available through the EXFOR database.]

References

1. R. Reifarth, C. Lederer, F. Käppeler, Neutron reactions in astrophysics. J. Phys. G Nucl. Phys. **41**(5), 053101 (2014)
2. M. Pignatari, K. Göbel, R. Reifarth, C. Travaglio, The production of proton-rich isotopes beyond iron: The γ-process in stars. Int. J. Modern Phys. E **25**(4), 1630003 (2016)
3. M. Arnould, S. Goriely, The p-process of stellar nucleosynthesis: astrophysics and nuclear physics status. Phys. Rep. **384**(1–2), 1–84 (2003). https://doi.org/10.1016/S0370-1573(03)00242-4
4. C. Travaglio, F.K. Röpke, R. Gallino, W. Hillebrandt, Type IA supernovae as sites of the p-process: two-dimensional models coupled to nucleosynthesis. Astrophys. J. **739**(2), 93 (2011). https://doi.org/10.1088/0004-637x/739/2/93
5. J. Bliss, A. Arcones, Y.-Z. Qian, Production of Mo and Ru isotopes in neutrino-driven winds: Implications for solar abundances and presolar grains. Astrophys. J. **866**(2), 105 (2018). https://doi.org/10.3847/1538-4357/aade8d
6. T. Rauscher, A. Heger, R.D. Hoffman, S.E. Woosley, Nucleosynthesis in massive stars with improved nuclear and stellar physics. Astrophys. J. **576**(1), 323–348 (2002). https://doi.org/10.1086/341728

7. C. Fröhlich, G. Martínez-Pinedo, M. Liebendörfer, F.-K. Thielemann, E. Bravo, W.R. Hix, K. Langanke, N.T. Zinner, Neutrino-induced nucleosynthesis of a>64 nuclei: The νp process. Phys. Rev. Lett. **96**, 142502 (2006). https://doi.org/10.1103/PhysRevLett.96.142502
8. K. Göbel, J. Glorius, A. Koloczek, M. Pignatari, R. Reifarth, R. Schach, K. Sonnabend, Nucleosynthesis simulations for the production of the p-nuclei ^{92}Mo and ^{94}Mo in a Supernova type II model. EPJ Web of Conf. **93**, 03006 (2015). https://doi.org/10.1051/epjconf/20159303006
9. T. Rauscher, N. Dauphas, I. Dillmann, C. Fröhlich, Z. Fülöp, G. Gyürky, Constraining the astrophysical origin of the p-nuclei through nuclear physics and meteoritic data. Rep. Progress Phys. **76**(6), 066201 (2013). https://doi.org/10.1088/0034-4885/76/6/066201
10. Reifarth, R., Göbel, K.: p-process fluxes. https://exp-astro.de/fluxes/ (2020)
11. C.E. Laird, D. Flynn, R.L. Hershberger, F. Gabbard, Proton-^{90}Zr interaction at sub-Coulomb proton energies. Phys. Rev. C **35**(4), 1265–1274 (1987). https://doi.org/10.1103/PhysRevC.35.1265
12. N.A. Roughton, M.R. Fritts, R.J. Peterson, C.S. Zaidins, C.J. Hansen, Thick-target measurements and astrophysical thermonuclear reaction rates: proton-induced reactions. Atomic Data Nucl. Data Tables **23**(2), 177–194 (1979). https://doi.org/10.1016/0092-640X(79)90004-4
13. Spyrou, A., Quinn, S.J., Simon, A., Rauscher, T., Battaglia, A., Best, A., Bucher, B., Couder, M., DeYoung, P.A., Dombos, A.C., Fang, X., Görres, J., Kontos, A., Li, Q., Lin, L.Y., Long, A., Lyons, S., Meyer, B.S., Roberts, A., Robertson, D., Smith, K., Smith, M.K., Stech, E., Stefanek, B., Tan, W.P., Tang, X.D., Wiescher, M.: Measurement of the ^{90,92}Zr(p,γ)^{91,93}Nb reactions for the nucleosynthesis of elements near A=90. Phys. Rev. C 88(4), 045802 (2013) arXiv:1310.5667 [nucl-ex]. https://doi.org/10.1103/PhysRevC.88.045802
14. T. Rauscher, F. Thielemann, Tables of nuclear cross sections and reaction rates: an addendum to the paper "Astrophysical reaction rates From statistical model calculations". Atomic Data Nucl Data Tables **79**(1), 47–64 (2001). https://doi.org/10.1006/adnd.2001.0863
15. L. Netterdon, V. Derya, J. Endres, C. Fransen, A. Hennig, J. Mayer, C. Müller-Gatermann, A. Sauerwein, P. Scholz, M. Spieker, A. Zilges, The γ-ray spectrometer horus and its applications for nuclear astrophysics. Nucl. Instruments Methods Phys Res Sect A Accelerators Spectrometers Detectors Associated Equipment **754**, 94 (2014). https://doi.org/10.1016/j.nima.2014.04.025
16. Mayer, M.: SIMNRA, a simulation program for the analysis of NRA, RBS and ERDA. AIP Conference Proceedings **475**(1) (1999). https://doi.org/10.1063/1.59188
17. J. Brenneisen, D. Grathwohl, M. Lickert, R. Ott, H. Röpke, J. Schmälzlin, P. Siedle, B.H. Wildenthal, The structure of ^{28}si above 10 Mev excitation energy i: gamma-decay modes and radiative widths of levels. Zeitschrift für Physik A Hadrons and Nuclei **352**(2), 149–159 (1995). https://doi.org/10.1007/BF01298901
18. L. Netterdon, V. Derya, J. Endres, C. Fransen, A. Hennig, J. Mayer, C. Müller-Gatermann, A. Sauerwein, P. Scholz, M. Spieker, A. Zilges, The γ-ray spectrometer horus and its applications for nuclear astrophysics. Nucl. Instruments Methods Phys. Res. Sect. A: Accelerators, Spectrometers, Detectors Associated Equipment **754**, 94–100 (2014). https://doi.org/10.1016/j.nima.2014.04.025
19. S. Agostinelli, J. Allison, K. Amako, J. Apostolakis, H. Araujo, P. Arce, M. Asai, D. Axen, S. Banerjee, G. Barrand, F. Behner, L. Bellagamba, J. Boudreau, L. Broglia, A. Brunengo, H. Burkhardt, S. Chauvie, J. Chuma, R. Chytracek, G. Cooperman, G. Cosmo, P. Degtyarenko, A. Dell'Acqua, G. Depaola, D. Dietrich, R. Enami, A. Feliciello, C. Ferguson, H. Fesefeldt, G. Folger, F. Foppiano, A. Forti, S. Garelli, S. Giani, R. Giannitrapani, D. Gibin, J.J.G. Cadenas, I. González, G.G. Abril, G. Greeniaus, W. Greiner, V. Grichine, A. Grossheim, S. Guatelli, P. Gumplinger, R. Hamatsu, K. Hashimoto, H. Hasui, A. Heikkinen, A. Howard, V. Ivanchenko, A. Johnson, F.W. Jones, J. Kallenbach, N. Kanaya, M. Kawabata, Y. Kawabata, M. Kawaguti, S. Kelner, P. Kent, A. Kimura, T. Kodama, R. Kokoulin, M. Kossov, H. Kurashige, E. Lamanna, T. Lampén, V. Lara, V. Lefebure, F. Lei, M. Liendl, W. Lockman, F. Longo, S. Magni, M. Maire, E. Medernach, K. Minamimoto, P.M. de Freitas, Y. Morita, K. Murakami, M. Nagamatu, R. Nartallo, P. Nieminen, T. Nishimura, K. Ohtsubo, M. Okamura, S. O'Neale, Y. Oohata, K. Paech, J. Perl, A. Pfeiffer, M.G. Pia, F. Ranjard, A. Rybin, S. Sadilov, E.D. Salvo, G. Santin, T. Sasaki, N. Savvas, Y. Sawada, S. Scherer, S. Sei, V. Sirotenko, D. Smith, N. Starkov, H. Stoecker, J. Sulkimo, M. Takahata, S. Tanaka, E. Tcherniaev, E.S. Tehrani, M. Tropeano, P. Truscott, H. Uno, L. Urban, P. Urban, M. Verderi, A. Walkden, W. Wander, H. Weber, J.P. Wellisch, T. Wenaus, D.C. Williams, D. Wright, T. Yamada, H. Yoshida, D. Zschiesche, Geant4-a simulation toolkit. Nuclear Instruments and Methods in Physics Research Section A: Accelerators, Spectrometers, Detectors and Associated Equipment **506**(3), 250–303 (2003). https://doi.org/10.1016/S0168-9002(03)01368-8
20. J.F. Ziegler, M.D. Ziegler, J.P. Biersack, SRIM - The stopping and range of ions in matter (2010). Nucl. Instruments Methods Phys. Res. B **268**(11–12), 1818–1823 (2010). https://doi.org/10.1016/j.nimb.2010.02.091
21. C.M. Baglin, Nuclear data sheets for a = 91. Nucl. Data Sheets **114**(10), 1293–1495 (2013). https://doi.org/10.1016/j.nds.2013.10.002
22. F. Bečvář, Simulation of γ cascades in complex nuclei with emphasis on assessment of uncertainties of cascade-related quantities. Nucl. Instruments Methods Phys. Res. Sect. A **417**(2), 434–449 (1998). https://doi.org/10.1016/S0168-9002(98)00787-6
23. User Manual. (2020). http://www.talys.eu